ELSEVIER

Journal of Alloys and Compounds 293–295 (1999) 601–607

Journal of ALLOYS AND COMPOUNDS

The effect of annealing on the discharge characteristics of $ZrV_{0.7}Mn_{0.5}Ni_{1.2}$ alloy

Sang-Min Lee*, Ji-Sang Yu, Ho Lee, Kuk-Jin Jang, Jai-Young Lee

Department of Materials Science and Engineering, Korea Advanced Institute of Science and Technology, 373-1 Kusong-Dong, Yusong-Gu, Taejon, South Korea

Abstract

In order to improve the discharge performance of the $ZrV_{0.7}Mn_{0.5}Ni_{1.2}$ alloy electrode, the alloy was annealed at 1000°C for 12 h. It is shown that total hydrogen storage capacity is unchanged, but the plateau pressure is increased in the lower hydrogen concentration range of the P–C–T curve after annealing. The annealed alloy has a higher rate capability and higher discharge capacity than the as-cast one. In order to analyze the above phenomena, the reaction surface area and surface reaction kinetics were examined by BET and EIS analyses, respectively. The measurement of the fully activated electrode surface area by BET analysis shows that there is little difference between as-cast and annealed alloy. The higher rate capability is due to the decrease of charge transfer resistance for the hydrogenation reaction in KOH electrolyte after annealing. It is well known that the Ni component plays a role in improving the electrocatalytic activity of the alloy electrode. The microstructures of the as-cast and annealed alloys were investigated by SEM and EDS analyses. The second phase (Zr–Ni phase) is widely distributed in the as-cast alloy, but this second phase disappears after annealing, resulting in homogenizing of the alloy and increasing Ni content in the matrix. The annealed alloy has a higher exchange current density than any single phase of the as-cast alloy. Consequently, it is concluded that the improved rate capability of the annealed alloy is due to increased Ni content in the matrix resulting from the disappearance of the secondary phase.

Keywords: Metal Hydride; Reversible hydrogen storage capacity; Rate-capability; Electrocatalytic activity

1. Introduction

Nickel-metal hydride (Ni-MH) batteries using hydrogen storage alloys as the negative electrode have been developed and commercialized to meet strong market demand for a power source with high energy density, high rate capability, long cycle life, and better environmental compatibility. A number of metals, alloys, and intermetallic compounds capable of forming hydrides have been studied extensively as potential electrodes, among which the rare earth metal-based and Ti or Zr-based alloys are considered to be most promising [1,2]. However, rare earth metal and Ti-based alloys are limited in developing high-capacity and high-performance Ni/MH batteries, because each alloy has a small discharge capacity and poor cycle life, respectively [3].

The $ZrV_{0.7}Mn_{0.5}Ni_{1.2}$ hydrogen storage alloy is attractive for an anode material in Ni/MH secondary batteries because of its large hydrogen storage capacity in gas–solid reactions and long cycling life in KOH electrolyte. However, this alloy has a low reversible hydrogen storage capacity because of large sloping characteristics in the P–C–T curve. A flat plateau pressure in the P–C–T curve of a hydrogen storage alloy is important for the performance characteristics such as discharge efficiency and discharge capacity because it is a direct determinant of reversible hydrogen storage capacity and discharge potential [4]. Therefore, it is necessary to flatten the plateau pressure region of the P–C–T curve of this alloy for developing a high-capacity and high-performance MH electrode. In order to improve the P–C–T characteristics of a hydrogen storage alloy, the strategy of substituting alternative alloy elements has been popular. However, this strategy is not entirely suitable for simultaneously improving the P–C–T characteristics. Recently, it has been reported that an annealing process is effective for reducing the slope of the PCT curve without degrading other P–C–T characteristics [5]. K. Morii et al. have studied the annealing effect on a Zr–Ti–V–Mn–Ni hydrogen storage alloy and found that the sloping characteristics of this alloy were improved, T. Sakai et al. have also found that the electrode from an annealed $MmNi_{3.5}Co_{0.8}Mn_{0.4}Al_{0.3}$ alloy

*Corresponding author.

0925-8388/99/$ – see front matter
PII: S0925-8388(99)00351-5

has a longer cycle life than that of an as-cast one, but the effect of annealing on electrode characteristics is not clearly understood [6,7]. Moreover, the previous studies did not pay attention to the effect of annealing on the discharge characteristics of the electrode.

In this work, the annealing process was applied to a $ZrV_{0.7}Mn_{0.5}Ni_{1.2}$ alloy. As a result of this process, changes of the thermodynamics and electrochemical properties of the alloy have been investigated. Finally, the effect of the annealing process on the discharge characteristics of this alloy will be discussed on the basis of electrochemical and phenomenological analyses.

2. Experimental

The base alloy was prepared in an arc-melting furnace under an argon atmosphere. The purity of the metals was at least 99.5 weight percent (wt.%). To assure the homogeneity of the alloy, the alloy ingot was turned over and remelted at least five times. Some samples from the base alloy were vacuum annealed in an electric furnace for 12 h at $T=1273$ K. The samples were crushed and ground into a powder with a characteristic particle diameter of about 100 μm for measurement of P–C-Isotherms and a particle diameter less than 45 μm for electrochemical measurements, respectively. For the electrochemical measurement, electrodes were made by mixing the sieved powders with copper powder in a weight ratio of 5:1 and pressing this mixture at a pressure of 10^4 N m^{-2} to porous pellets having a diameter of 10 mm. The experimental cell for electrochemical measurements consisted of the working electrode (Metal Hydride electrode), the counter electrode (Pt wire) and a reference electrode (Hg/HgO electrode). The reference electrode was equipped with a Luggin probe to reduce the IR drop in the polarization measurements. The electrolyte was 30 wt.% KOH solution and its temperature was controlled at 30±1°C. The alloy electrode was galvanostatically charged at 50 mA g^{-1} for 10 h, and after resting for 5 min it was discharged at 100 mA g^{-1} until the potential reached −0.75 V vs. Hg/HgO. After full activation, electrochemical impedance spectra were recorded out under open-circuit conditions using a Solartron SI1255 frequency response analyzer and a EG&G 273A potentiostat. The impedance spectra of the electrodes were recorded in a frequency range from 10 KHz to 5 MHz and at 5 mV amplitude perturbation for various depths of discharge (DOD). It is shown that the kinetics of the charge-transfer reaction, i.e., the exchange current density, can be characterized electrochemically by changing potentiodynamically (1 mV s^{-1}) the overpotential within a small range ($\eta=\pm10$ mV) and measuring the current. The phase distribution of the alloy was analyzed by scanning electron microscopy (SEM) and its chemical composition was characterized by energy dispersive spectroscopy (EDS) analysis. The specific reaction area of the electrode was measured by BET method to determine the factors affecting the rate capability after annealing. In order to analyze the surface composition of the alloy after annealing, Auger electron spectroscopy (AES) analysis was performed. In AES analysis, a Perkin-Elmer PHI4300-SAM instrument having a base pressure of 1×10^{-9} Torr was used and depth profiling was performed by using Ar^+ ions at 3 kV for sputtering.

3. Results and discussion

Establishment of annealing condition – for improving the sloping characteristics of the P–C–T curve effectively, optimization of annealing conditions is necessary. Generally, annealing conditions affecting P–C–T characteristics are annealing time and temperature. First of all, optimization of annealing temperature is fixed at about 1000°C which is homologous temperature (0.5 T/T_m) of the alloy constituent element in view of homogenizing the alloy by diffusion after the annealing process. Fig. 1 shows the change of the P–C–T curve with annealing time (6–24 h). It is illustrated that the degree of improvement in sloping characteristics is saturated after 12 h. Therefore, it can be seen that annealing condition is optimized at 1000°C, for 12 h.

Measurement of P–C–T (Pressure–Composition)Isotherm curves – typical pressure–composition isotherms of the as-cast and annealed $ZrV_{0.7}Mn_{0.5}Ni_{1.2}$ alloy are illustrated in Fig. 2. It is seen that the total hydrogen storage capacity is unchanged, but a flatter region is formed in the low equilibrium hydrogen pressure range of

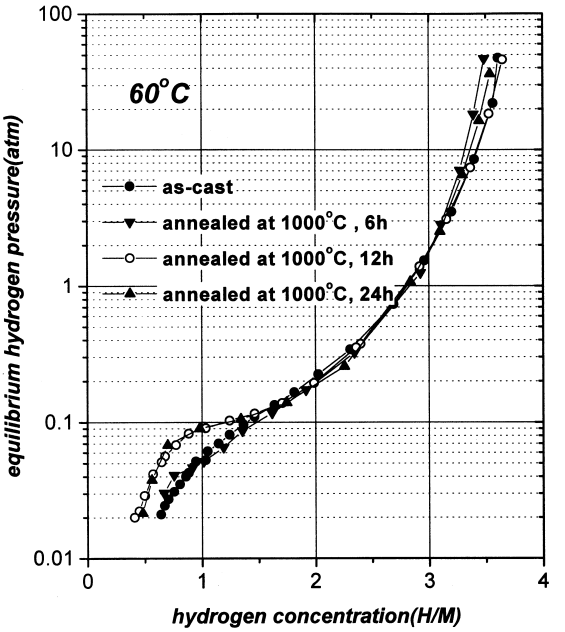

Fig. 1. The change of the P–C–T curve for the $ZrV_{0.7}Mn_{0.5}Ni_{1.2}$ alloy with annealing time (6–24 h).

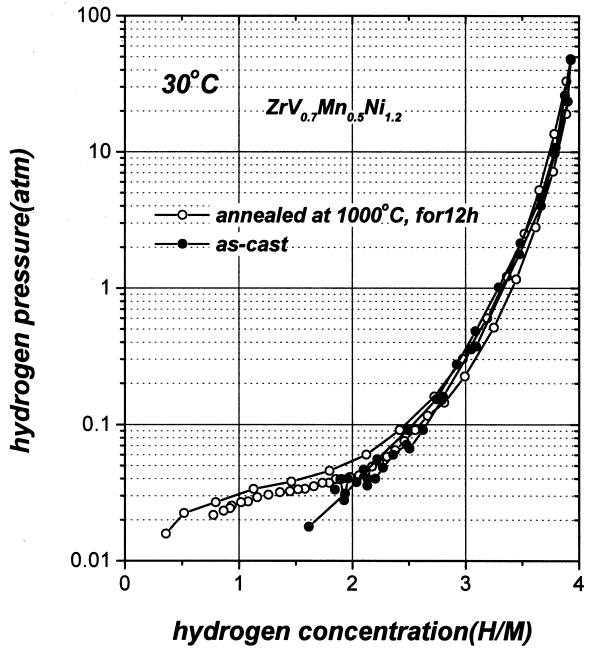

Fig. 2. P–C–T curves of the as-cast and annealed $ZrV_{0.7}Mn_{0.5}Ni_{1.2}$ alloys at 1000°C for 12 h.

the P–C–T curve after annealing. This phenomena indicates that the annealing process is effective for improving the sloping characteristics of the P–C–T curve, which implies an increased reversible hydrogen storage capacity absorbed in the 0.01–1 atm range of equilibrium hydrogen pressure.

Half cell test – Fig. 3(a) shows discharge curves of as-cast and annealed alloys at a discharge rate of 100 mA g^{-1}. The discharge capacity increased by 11% after annealing. Generally, the discharge capacity of the metal hydride electrode can be increased by improved rate capability or increased reversible hydrogen storage capacity in gas–solid reactions. It therefore should be determined which of these factors is the primary source of this additional discharge capacity. Fig. 3(b) shows the discharge curves of as-cast and annealed alloys at a low discharge rate of 25 mA g^{-1}. The discharge capacity is only slightly increased at a low discharge rate after annealing. As pointed out above, it may be concluded that the discharge capacity is increased not due to an increase of reversible hydrogen storage capacity, but instead due to an improvement in the rate capability of the electrode after annealing.

Measurements of rate capability – Fig. 4 shows the change of discharge capacity with increasing discharge current density. The discharge capacity ratio C/C_{max} is increased by 40% after annealing. In general, it is well known that electrode properties such as rate capability and discharge efficiency are strongly dependent on the surface reaction kinetics of the hydrogenation reaction in KOH solution [8,9]. Also the surface reaction kinetics are controlled primarily by surface catalytic activity, i.e. exchange current density and the specific reaction surface area are related as follows;

$$I_o = i_o \times S$$

where

I_o: surface reaction kinetics (i.e. exchange current; mA g^{-1})

i_o: surface catalytic activity (i.e. exchange current density; mA cm^{-2})

S: specific reaction surface area (m^2 g^{-1}).

In order to identify the major factor responsible for improving the rate capability of the alloy electrode after annealing, the specific reaction surface area (S) and surface catalytic activity (i_o) were measured, respectively.

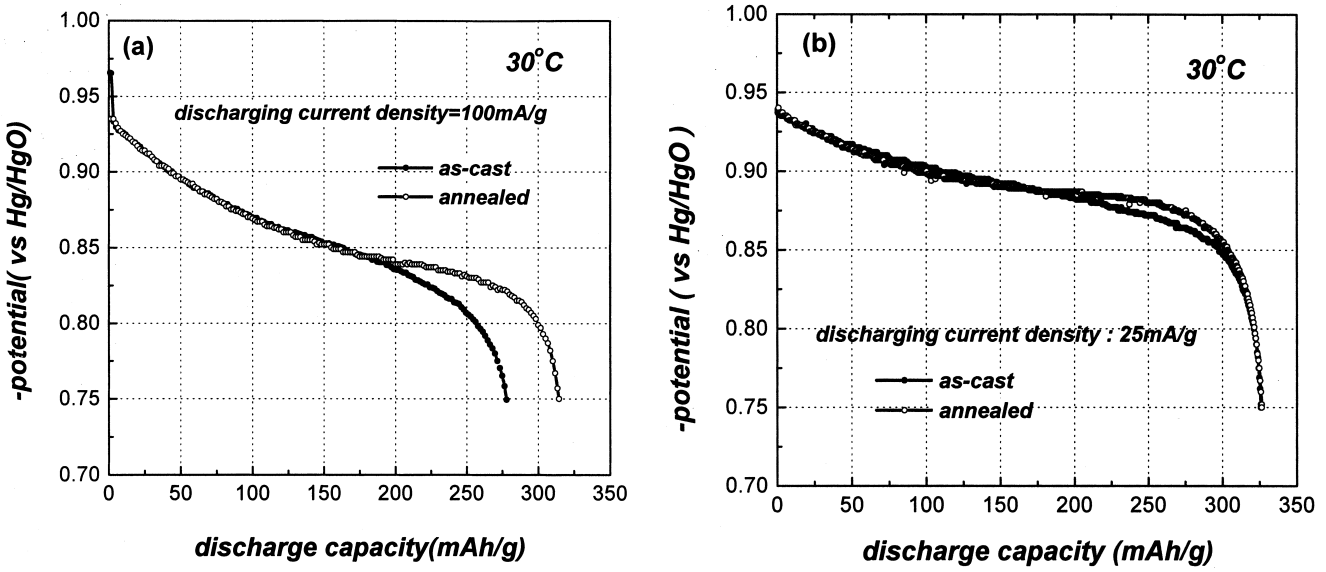

Fig. 3. (a) Discharge curves of as-cast and annealed $ZrV_{0.7}Mn_{0.5}Ni_{1.2}$ alloys at a discharge current density of 100 mA g^{-1}; (b) at 25 mA g^{-1}.

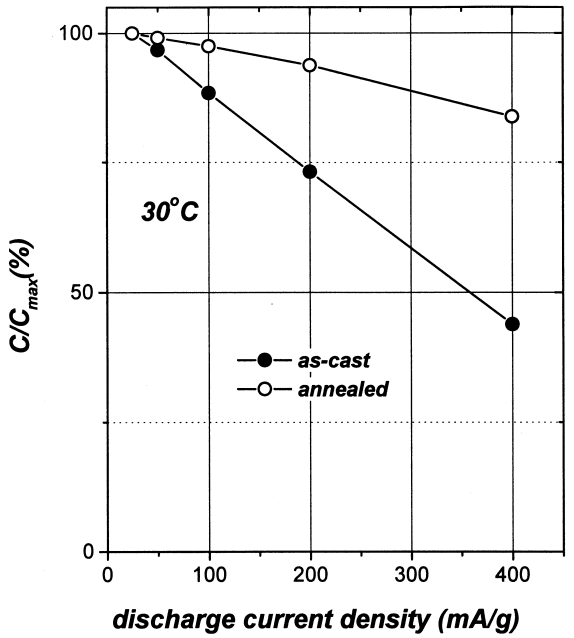

Fig. 4. Current dependences of discharge capacity at 30°C of as-cast and annealed $ZrV_{0.7}Mn_{0.5}Ni_{1.2}$ alloys.

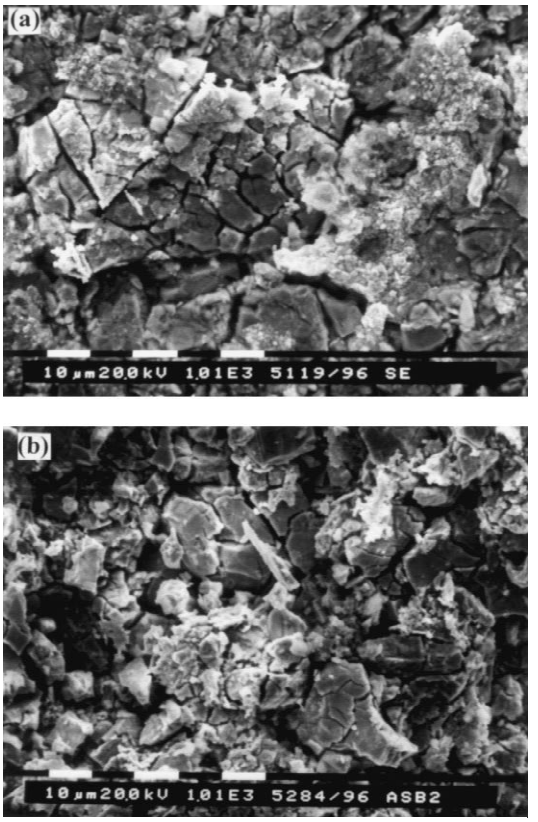

Fig. 5. Surface morphologies of (a) as-cast and (b) annealed alloy electrodes after full activation.

Measurement of surface area – electrochemical cycling, i.e., the hydrogen charging and discharging processes in KOH electrolyte, caused an increase in the number of fine cracks of the alloy electrode responsible for the change in the high-rate discharge capability. Fig. 5(a) and (b) show SEM photographs of the cross section of as-cast and annealed alloy electrodes after full activation. It is observed that there is no difference of the pulverization degree between the two electrodes. Moreover, BET analysis clearly shows that the specific reaction surface area of the electrode is little changed after annealing (as-cast: 4.02 $m^2\ g^{-1}$, annealed: 3.86 $m^2\ g^{-1}$). From the above results, it is evident that the improvement of rate capability after annealing cannot be explained by the change of reaction surface area.

Electrochemical Impedance Spectroscopy analysis – the impedance spectra of as-cast and annealed alloy electrodes from 10 KHz to 5 MHz at the various depths of discharge (DOD) are shown in Fig. 6(a) and (b). The smaller semicircle in the high-frequency region is barely changed, but the semicircle in the low-frequency region is changed markedly with DOD. It is clear that the rate-controlling step for the electrode reaction is the charge transfer resistance for the hydrogenation reaction in KOH electrolyte. The reaction resistance from the semicircle in the low-frequency region can be calculated by a complex non-linear least square (CNLS) fitting program. The DOD dependence of the charge transfer resistance for two electrodes is illustrated in Fig. 7. The charge transfer resistance is decreased significantly irrespective of the change of hydrogen content in the electrode after annealing. It is found that catalytic activity per unit area of the alloy electrode is obviously increased after annealing.

Alloy surface composition analysis – the electrochemical reaction process always takes place on the alloy/solution interface. Moreover, it is well known that the catalytic activity of the alloy is closely limited to the presence of elemental Ni, which acts as an electrocatalyst for the hydrogen evolution reaction. Therefore, it is important to obtain information about the alloy surface composition. The change of alloy surface composition after annealing is shown in Fig. 8. The Ni content of the alloy surface region is increased after annealing. Generally, rate capability depends on the Ni concentration in the surface region of the alloy electrode after full activation. The difference of the relative Ni amount in the electrode surface before cycling between as-cast and annealed alloy samples can be maintained even after full activation [10]. Therefore, it can be considered that increased Ni concentration in the alloy surface region is responsible for improving the rate capability of the annealed alloy electrode. In order to identify the source of increasing Ni concentration in the surface region, the change of Ni concentration in the matrix after annealing should be examined.

Phase analysis – a cross-sectional view imaged by

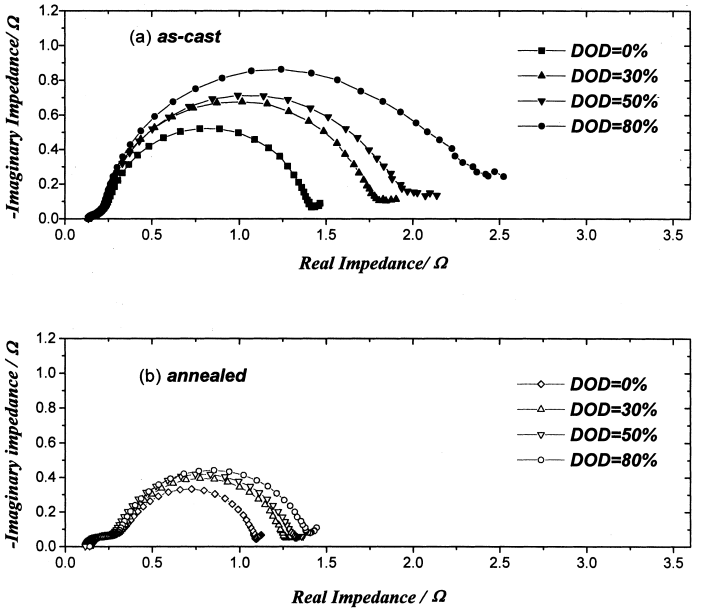

Fig. 6. Cole–Cole plots at various applied DOD = 0, 30, 50, and 80% for (a) as-cast and (b) annealed $ZrV_{0.7}Mn_{0.5}Ni_{1.2}$ alloy electrodes after full activation.

scanning electron microscopy shows that secondary phases are uniformly distributed over the as-cast alloy and disappear into the matrix after annealing (Fig. 9). Compositional analysis by EDS shows that the Ni content of the matrix is increased, as the microstructure of this alloy is homogenized after annealing (Table 1). On the basis of phenomenological analysis, it can be concluded that the Ni content in the matrix is increased, which is due to the

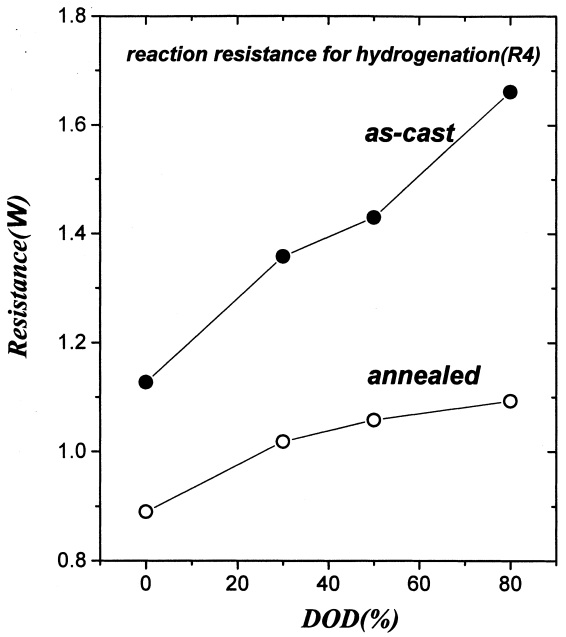

Fig. 7. Variations of charge transfer resistance with DOD = 0, 30, 50, and 80% for as-cast and annealed alloy electrodes.

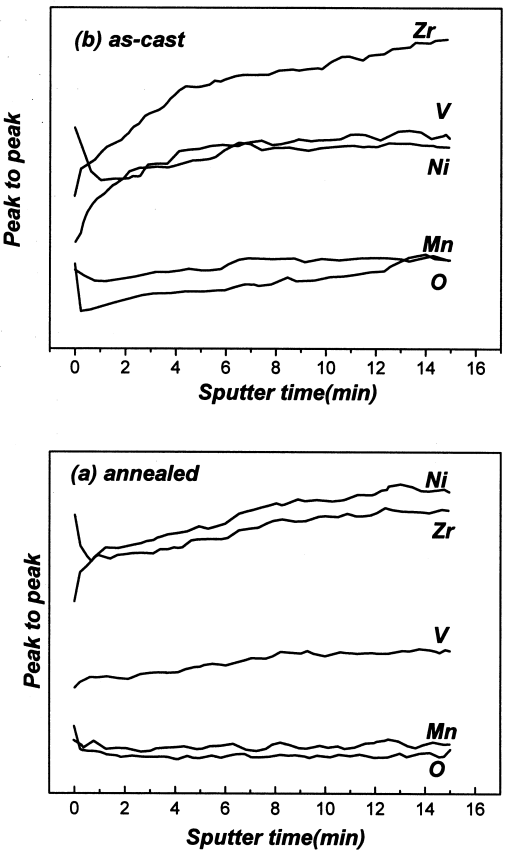

Fig. 8. AES depth profiles for the constituent elements of (a) as-cast and (b) annealed $ZrV_{0.7}Mn_{0.5}Ni_{1.2}$ alloy electrodes before electrochemical charge/discharge cycling.

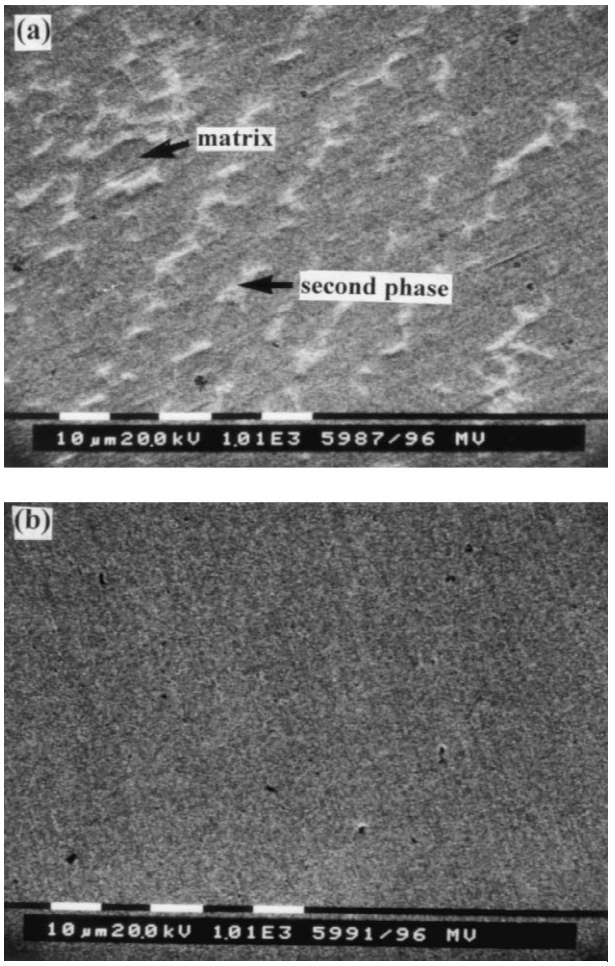

Fig. 9. Microstructure of (a) the as-cast and (b) annealed $ZrV_{0.7}Mn_{0.5}Ni_{1.2}$ alloys.

disappearance of a secondary phase (Zr–Ni phase) after annealing.

The role of each phase – Fig. 10 shows the change of discharge capacity with increasing discharge current density for each phase prepared, on the basis of EDS analysis. The rate capability of the secondary phase is higher than that of the as-cast alloy. This shows that the improved rate capability of the annealed alloy is not affected by the disappearance of secondary phase, in itself. In order to clarify these suggestions, the exchange current density of each phase was measured as a barometer of electrocatalytic activity (Fig. 11). Of all phases, the annealed alloy has the highest exchange current density. Therefore, it is suggested that improvement in rate capability of this alloy after

Table1
The result of EDS analysis of each phase in annealed and as-cast alloys

	As-cast alloy	Annealed alloy
Matrix	$ZrV_{0.73}Mn_{0.49}Ni_{0.95}$	$ZrV_{0.75}Mn_{0.52}Ni_{1.25}$
Secondary phase	$ZrV_{0.11}Mn_{0.10}Ni_{1.04}$ (Zr–Ni)	–

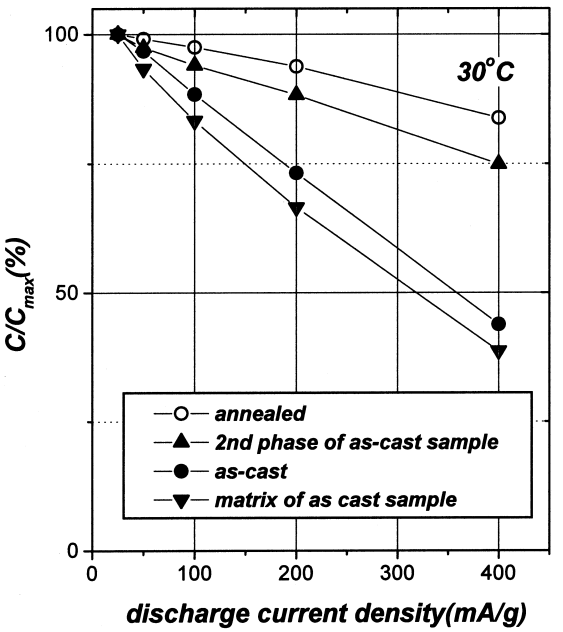

Fig. 10. Current dependence of discharge capacity for electrodes of each phase identified with EDS analysis.

annealing is due to increased Ni content in the matrix resulting from the disappearance of the secondary phase.

4. Conclusion

The $ZrV_{0.7}Mn_{0.5}Ni_{1.2}$ alloy has been annealed for 12 h at 1000°C to flatten the plateau region of the P–C–T curve. The annealed alloy has a higher rate capability and

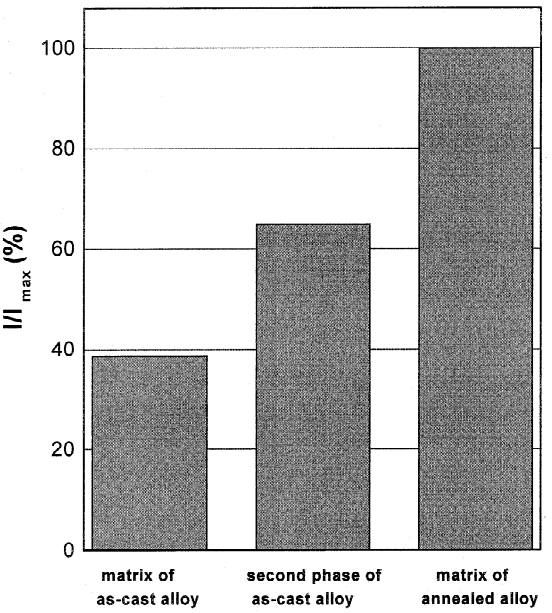

Fig. 11. Exchange current density at DOD=50% for the electrode of each phase identified with EDS analysis.

discharge capacity than the as-cast alloy. Measuring the electrode surface area by BET analysis shows that the surface area for a fully activated electrode of this alloy is little changed after annealing. However, it is found that catalytic activity per unit area of alloy electrode is significantly increased after annealing as determined by EIS analysis. A cross sectional view of the electrode by SEM shows that the second phase (Zr–Ni phase) is uniformly distributed over the as-cast alloy and disappears into the matrix after annealing. The increase of the Ni content in the matrix after annealing results in an increase of the electrocatalytic activity for the hydrogenation reaction of the alloy in KOH electrolyte. Overall, the improvement in the rate capability of the annealed alloy is due to increased Ni content in the matrix.

Acknowledgements

This work was supported by the hydrogen energy research center, KAIST.

References

[1] J.J. Willems, K.H.J. Buschow, J. Less-Common Metals 129 (1987) 13.
[2] M.A. Fetchenko, S. Venkatesan, K.C. Hong, B. Beichman, Power Sources 12 (1989) 411.
[3] H.H. Lee, J.Y. Lee, J. Alloys Comp. 253 (1997) 601.
[4] M.H.J. Van Rijswick, Proceedings of the International Symposium on Hydrides for Energy Storage, Ge: 10, Norway 261, (1977).
[5] H. Nakamura, Y. Nakmura, S. Fujitani, I. Yonezu, J. Alloys Comp. 218 (1995) 216.
[6] K. Morii, T. Shimizu, J. Alloys Comp. 231 (1995) 524.
[7] T. Sakai, H. Miyamura, N. Kuriyama, H. Ishikawa, I. Uehara, Z. Phys. Chem. 183 (1994) 333.
[8] M. Tatokoro, K. Moriwaki, K. Nishio, M. Nogami, N. Inoue, Electochemical Society Proceeding, 92-5, (1992).
[9] D.M. Kim, J.H. Jung, H.H. Lee, J.Y. Lee, J. Korean Hydrogen Energy Soc. 7, No. 1 (1996).
[10] S.R. Kim, K.Y. Lee, J.Y. Lee, J. Alloys Comp. 223 (1995) 22.